Supplement of Biogeosciences, 22, 2181–2200, 2025
https://doi.org/10.5194/bg-22-2181-2025-supplement

Biogeosciences Open Access EGU

Supplement of

Modeling the contribution of micronekton diel vertical migrations to carbon export in the mesopelagic zone

Hélène Thibault et al.

Correspondence to: Hélène Thibault (helene.thibault@mio.osupytheas.fr)

Contents

S1 Bioenergetic model

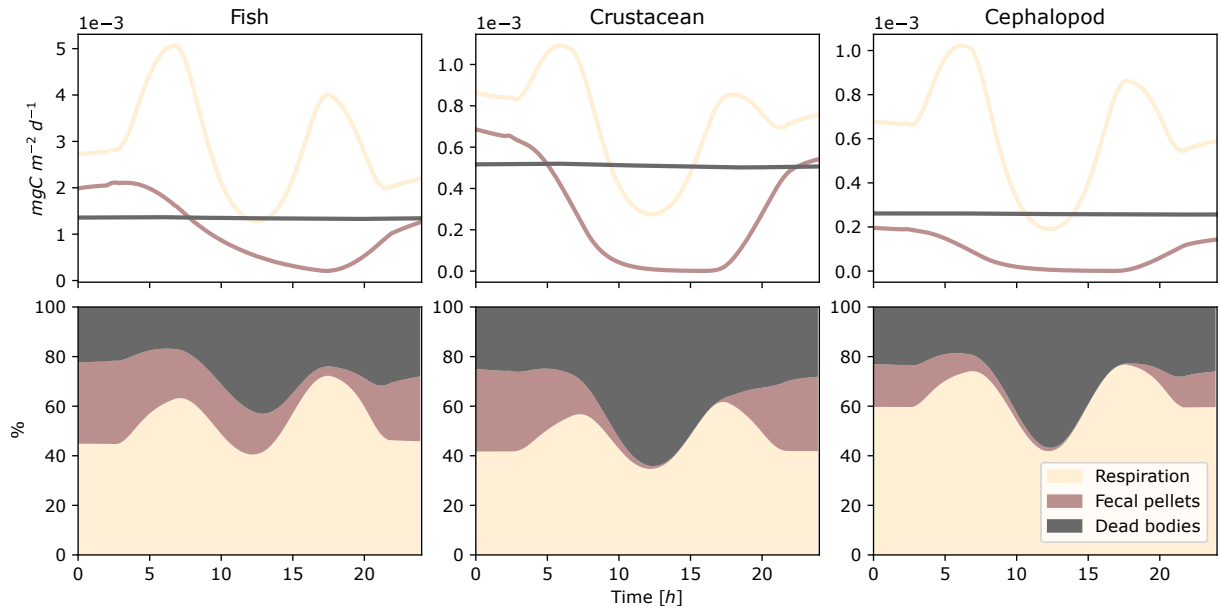

Figure S1: Daily variation of carbon production including metabolic products (D_m), fecal pellets (D_g) and dead bodies (D_μ) for the three taxonomic groups (Fish, Crustacean, Cephalopod). The absolute variation (top panels) and the relative variation of all the carbon products (bottom panels) are a daily mean of the five different sizes of each taxonomic groups, as represented in Fig.3.

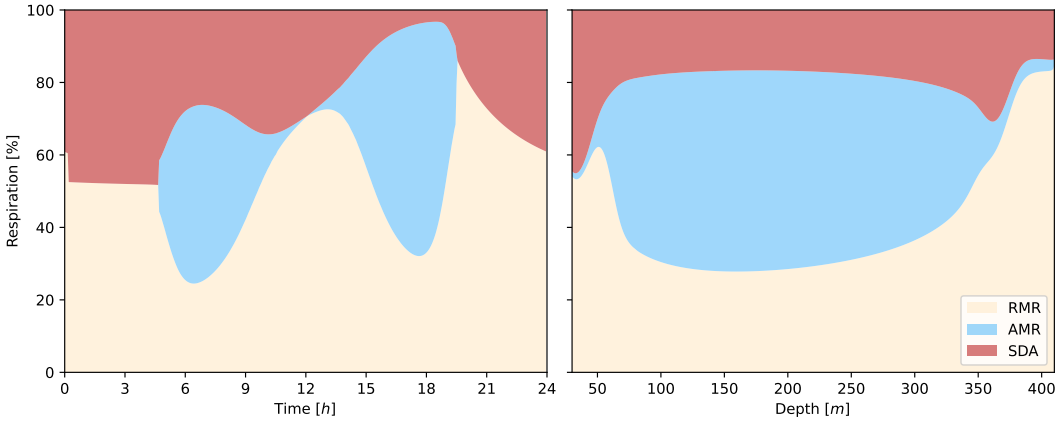

Figure S2: Relative importance of the respiration rates depending on micronekton activity: resting (RMR), swimming (AMR) and feeding (SDA). The parameters of this simulation correspond to a fish of 35mm.

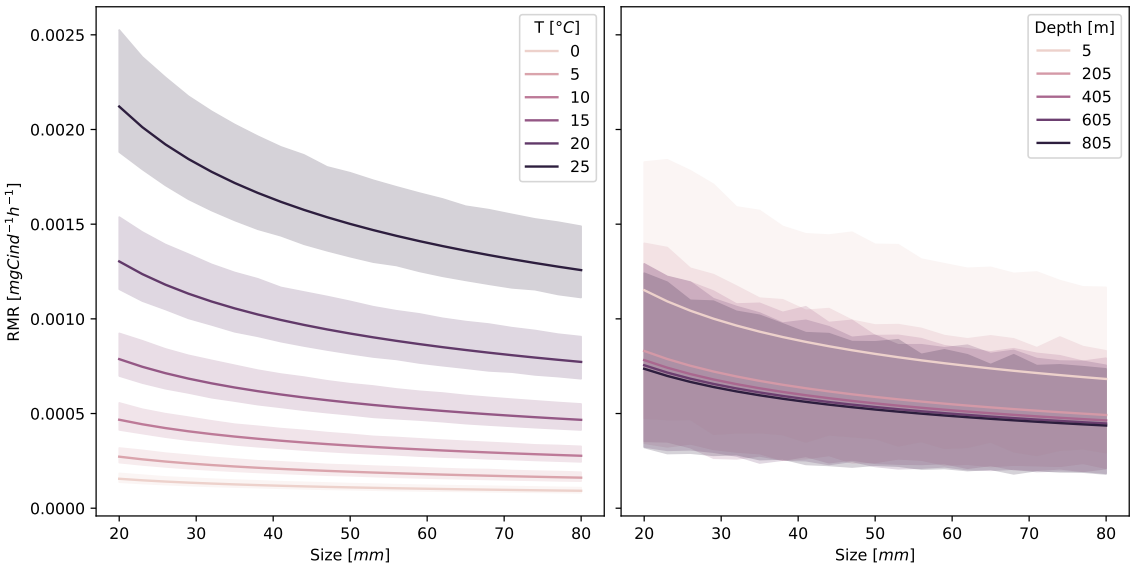

Figure S3: Routine respiration rates (RMR) as a function of size, temperature and depth. Here as an example for a fish from Eq.5.

Detritus pools (%)	Fish	Crustacean	Cephalopod
D_m	53.9±8.7	46.5±8.2	61.8±10.8
$D_m > 200m$	54.7±12.9	49.6±10.6	56.5±17.0
D_g	22.3±1.3	20.1±2.4	9.2±1.8
$D_g > 200m$	16.3±0.9	3.2±1.2	2.3±1.1
D_μ	23.8±10.0	33.1±10.7	29.0±12.6
$D_\mu > 200m$	29.0±13.8	47.2±12.0	41.1±18.1

Table S1: Summary statistics of the relative contribution of the carbon detritus including metabolic products (D_m), fecal pellets (D_g) and dead bodies (D_μ) produced by micronekton of different sizes. This represents mean values of the integrated daily production along the water column and under 200 m depth, associated with their standard deviation. These values correspond to those represented in Fig.4.

Table S2: Respiration coefficients used to calculate respiration rates for the different taxonomic groups: Fish (F), Crustacean (A) and Cephalopod (S). Mean values correspond to those used in the simulations as indicated in Table 2 and the standard error (std) was added to or subtracted from the mean to define the range of these parameters for the sensitivity analysis.

Symbol	Mean (std)	Group	Source
a_0	30.767 (2.451)	F	Ikeda (2016)
a_1	0.870 (0.020)	F	Ikeda (2016)
a_2	-8.515 (0.737)	F	Ikeda (2016)
a_3	-0.088 (0.031)	F	Ikeda (2016)
a_0	24.461 (5.820)	S	Ikeda (2016)
a_1	0.868 (0.054)	S	Ikeda (2016)
a_2	-6.424 (1.650)	S	Ikeda (2016)
a_3	-0.261 (0.064)	S	Ikeda (2016)
a_0	23.079 (0.970)	A	Ikeda (2014)
a_1	0.813 (0.013)	A	Ikeda (2014)
a_2	-6.248 (0.280)	A	Ikeda (2014)
a_3	-0.136 (0.011)	A	Ikeda (2014)

S2 Modeling irradiance

Surface irradiance (I_0 in Eq.2,4) was modeled as a periodic function of time t, varying over the day as follows,

$$I_0(t) = (I_{min} + I_{max}) - I_{max} \exp(-a\ sin^n(\omega t)) \tag{S1}$$

with $I_{min} = 0.01$ and $I_{max} = 1$, the minimum and maximum level of light, $\omega = (2\pi)/2H$ where H=24h, the parameter n=15, defining the timing of twilight hours, and the parameter $a = 4$ defining the degree of flattening of the curve (see an example in Fig.2).

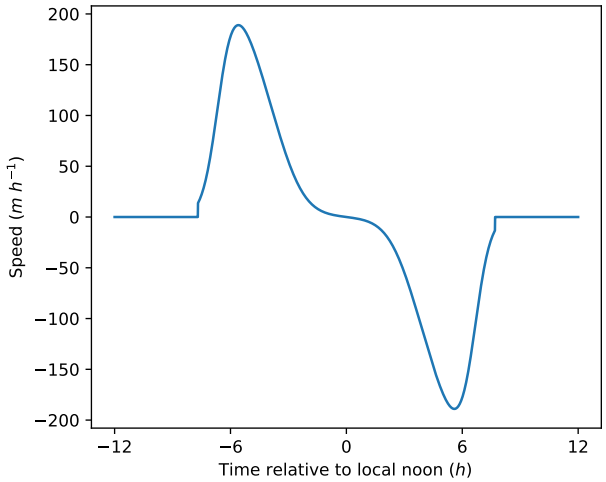

Figure S4: Relative daily migration speed for a fish measuring 35mm. A positive swimming speed causes organisms to go down to the bottom of the water column, and a negative speed causes them to rise to the surface.

The parameter n varies annually according to the time of sunrise and sunset, calibrated with the winter solstice in December, when days last 8 hours, and during the summer solstice in June, when daylight last 16 hours at PAP-SO,

$$n = (n_{max} - n_{min}) \frac{cos(\omega(t+T)+1)}{2 + n_{min}} \tag{S2}$$

with $\omega = (2\pi)/T$ where T=365 j, $n_{max} = 30$ and $n_{min} = 6$.

The annual surface irradiance was finally computed with the annual variation of the solar angle following the cosine law,

$$I_{year}(t, 0) = I_0(t) cos(\phi) \tag{S3}$$

where ϕ is the solar angle as a function of latitude, longitude and time of the year.

Annual irradiance along depth z was computed for the visual predation rate based in Eq.5,

$$I_{year}(t, z) = I_{year}(t, 0) e^{-K_{d490}(z).z} \tag{S4}$$

The attenuation coefficient was defined from the empirical equation of Morel et al. (2007),

$$\phi(z) = 0.0166 + 0.072\ Chl(z)^{0.69} \tag{S5}$$

where Chl is the chlorophyll a concentration along the water column in mg m^{-3} at PAP-SO, from Copernicus Marine Service Information (CMEMS).

S3 Relative effects of seasonal parameters

The relative influence of the three environmental factors on carbon production was investigated separately. This results in three simulations showed in Fig.S5, each varying one of the environmental factors over the year, the other two remaining stable over the seasons (Table.S3).

Scenarii	Seasonal variation			
	PP	Temp.	Light	c_α
Scenario 1	X			3
Scenario 2		X		0.7
Scenario 3			X	2
Scenario 4	X	X	X	7

Table S3: Seasonal simulations involving both independent and dependent variation of the environment conditions with the scaling coefficient c_α, used to calculate the visual capture rate in Eq.5.

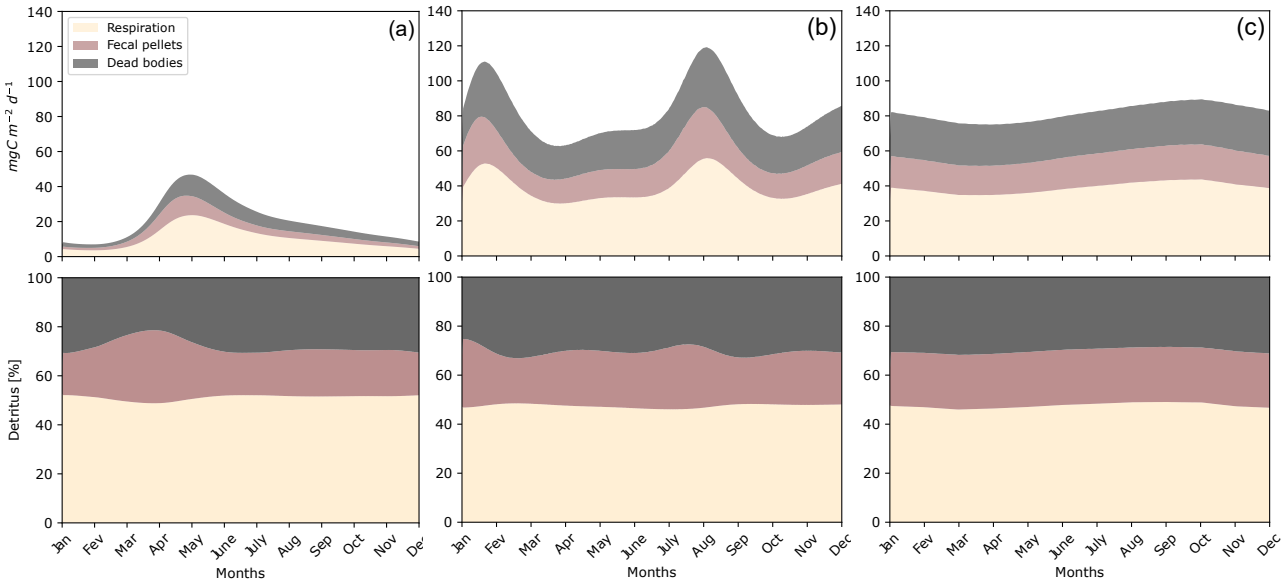

Figure S5: Daily carbon production over the year involving independently simulated seasonal variations for each environmental variable: phytoplankton concentration (a), light (b) and temperature (c). Carbon production is integrated along depth, including respiration (D_m), fecal pellets (D_g) and dead bodies (D_μ).

Seasonal variation of phytoplankton concentrations generated a strong peak of detritus production in May that reached 50 mgC m^{-2} d^{-1} (Fig.S5a). This peak then attenuated until it reached its lowest values in January, of 8 mgC m^{-2} d^{-1}. The proportion of the metabolic products changed slightly around 50%. The highest proportion of fecal pellets occurs just before the peak of production, around 30% of the total carbon production induced by micronekton and is around 20% the rest of the year.

Independent variation of light generated two peak of carbon production with one in February and another one in late summer of 120 mgC m^{-2} d^{-1} corresponding to maximum light intensity and shortest nights (Fig.S5b). This peaks of production are preceded by a higher proportion of fecal pellets around 30% compared to 20% the rest of the year.

Variation of temperature had a less pronounced effect than the phytoplankton concentration on detritus production with a maximum of 85 mgC m^{-2} d^{-1} in October and a minimum of 75 mgC m^{-2} d^{-1} in April (Fig.S5c). The proportions of the three different carbon detritus were stable during the year with a slight increase in the percentage of

respiration in summer. Respiration as DIC represented almost 50% of the total carbon production, fecal pellets 20% and dead bodies 30%.

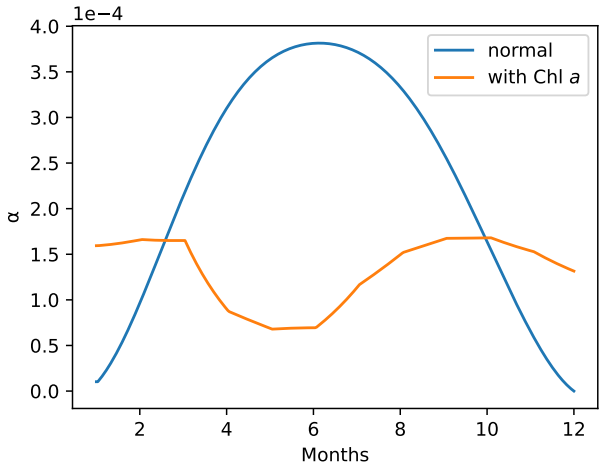

Figure S6: Variation of the capture rate α at 40 m over a year based on two environmental conditions. The blue curve corresponds to the computation of the capture rate from Eq.S4 and Eq.S5 with a constant attenuation coefficient, used for Fig.S5c. The orange curve corresponds to the computation of the capture rate with the attenuation coefficient, function of Chl *a* concentrations (Eq.SS5) used for Fig.7 and Fig.8.

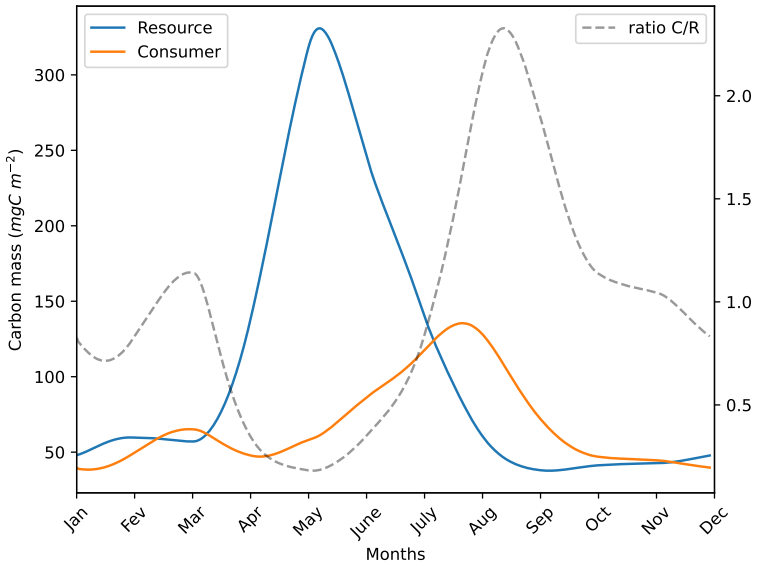

Figure S7: Carbon concentration of the resource (R) and the consumer (C) with environmental variations over the year. This corresponds to the simulation of the carbon production observed in Fig.7,8.

S4 Size and biomass distribution

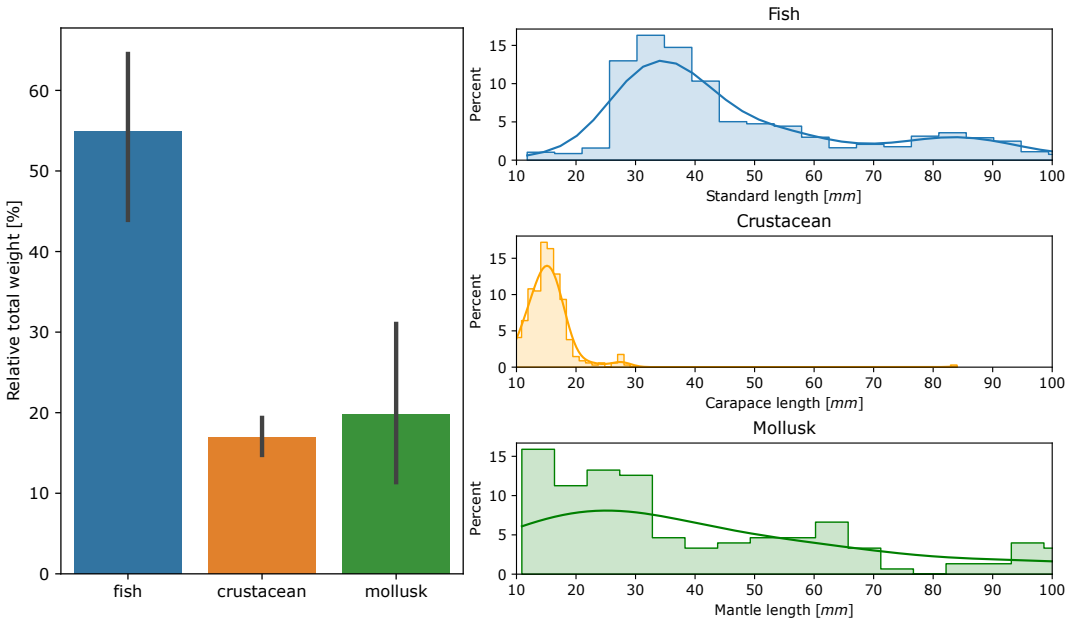

Figure S8: Weight and size distribution of three micronekton taxonomic groups (fish, crustacean and mollusk) collected with a mid-water trawl during the APERO cruise (com. pers.). The variability of the relative total weight comes from the differences between the stations.

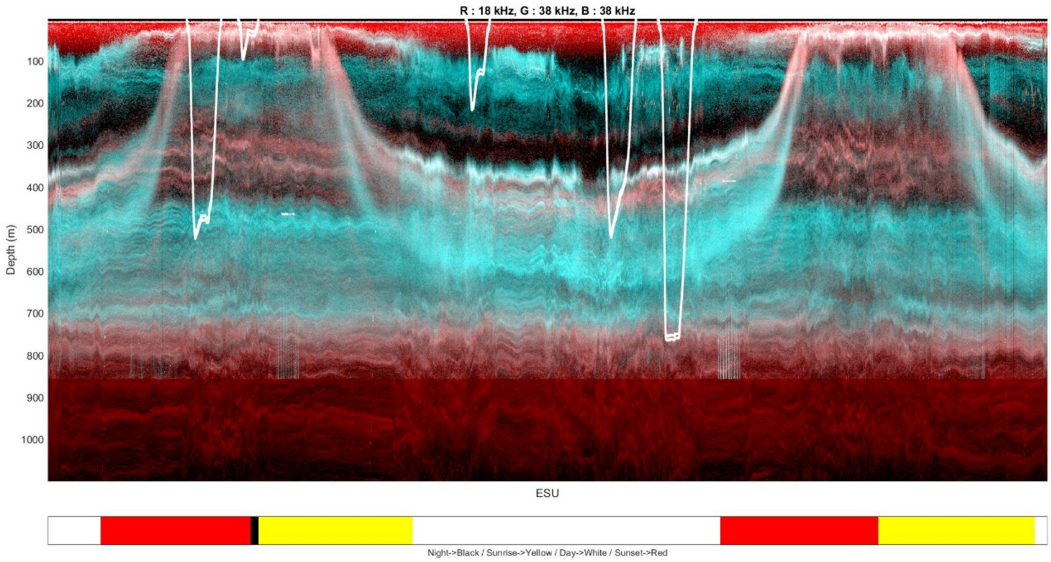

Figure S9: Example of an echogram for one station of the APERO cruise obtained from continuous acoustic measurements with a Simrad EK80 (com. pers.). This RGB composite image of Sv values (dB re 1 m^{-1}) represents two frequencies: 18 and 38 kHz, respectively in red and blue-green. The white lines correspond to the trajectory of the mid-water trawl deployed.

Fish		Crustacean		Cephalopod	
Size	c_α	Size	c_α	Size	c_α
20	4.9	10	7.1	20	2.4
35	3.3	20	4.6	35	2.1
50	2.9	30	3.7	50	2.1
65	2.7	40	3.3	65	2.1
80	2.7	50	3	80	2.1

Table S4: Scaling coefficient c_α, used to calculate the visual capture rate in Eq.5. for the size and taxonomic dependent simulations in Fig.3,4.

References

Ikeda, T.: Respiration and ammonia excretion by marine metazooplankton taxa: synthesis toward a global-bathymetric model, Marine biology, 161, 2753–2766, https://doi.org/10.1007/s00227-014-2540-5, 2014.

Ikeda, T.: Routine metabolic rates of pelagic marine fishes and cephalopods as a function of body mass, habitat temperature and habitat depth, Journal of Experimental Marine Biology and Ecology, 480, 74–86, https://doi.org/10.1016/j.jembe.2016.03.012, 2016.

Morel, A., Huot, Y., Gentili, B., Werdell, P. J., Hooker, S. B., and Franz, B. A.: Examining the consistency of products derived from various ocean color sensors in open ocean (Case 1) waters in the perspective of a multi-sensor approach, Remote Sensing of Environment, 111, 69–88, https://doi.org/10.1016/j.rse.2007.03.012, 2007.